

## Thermal Diffusivity of $\text{La}_{1-x}\text{Sr}_x\text{MnO}_3$ ( $x < 0.3$ )<sup>1</sup>

A. Salazar,<sup>2,3</sup> A. Oleaga,<sup>2</sup> and D. Prabhakaran<sup>4</sup>

---

Perovskite manganites are interesting because of their colossal magnetoresistance. In this work high resolution thermal diffusivity measurements of  $\text{La}_{1-x}\text{Sr}_x\text{MnO}_3$  ( $0 \leq x \leq 0.3$ ) single crystals in the temperature range from 250 to 400 K are presented. A photopyroelectric device in the standard back configuration has been used. The thermal diffusivity through second-order magnetic phase transitions, as well as through first- and second-order structural phase transitions has been measured. The critical parameters of the sample with  $x=0.3$  at the ferromagnetic-to-paramagnetic transition have been obtained, and are close to the values predicted by the Ising model.

---

**KEY WORDS:** critical parameters; manganites; phase transitions; photopyroelectric; thermal diffusivity.

### 1. INTRODUCTION

In recent years great attention has been paid to perovskite manganites  $\text{L}_{1-x}\text{A}_x\text{MnO}_3$  (L = lanthanide, A = alkaline earth) due to their colossal magnetoresistance, i.e., the large decrease of the electrical resistivity near the Curie temperature by applying a magnetic field [1, 2]. This effect is interesting for both basic research and potential technological applications, such as magnetic recording, actuators, and sensors. However, while many studies have been devoted to the study of their magnetic and electrical properties, only a few papers deal with their thermal transport properties.

---

<sup>1</sup>Paper presented at the Fifteenth Symposium on Thermophysical Properties, June 22–27, 2003, Boulder, Colorado, U.S.A.

<sup>2</sup>Departamento de Física Aplicada I, Escuela Superior de Ingenieros, Universidad del País Vasco, Alameda Urquijo s/n, 48013 Bilbao, Spain.

<sup>3</sup>To whom correspondence should be addressed. E-mail: wupsahea@bi.ehu.es

<sup>4</sup>Clarendon Laboratory, Department of Physics, University of Oxford, Oxford OX1 3PU, United Kingdom.

In this work we present high resolution thermal diffusivity measurements on a set of  $\text{La}_{1-x}\text{Sr}_x\text{MnO}_3$  ( $0 \leq x \leq 0.3$ ) single crystals using a photopyroelectric (PPE) device in the back configuration, where an opaque slab is periodically illuminated on one side, while the other side is in contact with the pyroelectric detector [3]. This technique is specially suited to the study of the through-thickness thermal properties around phase transitions, since small temperature gradients in the sample produce a good enough signal-to-noise ratio. Therefore, the thermal parameters close to the phase transition are measured with high accuracy [4, 5].

$\text{La}_{1-x}\text{Sr}_x\text{MnO}_3$  materials have a very complicated behavior, where magnetic, electronic, and structural phase transitions take place [6–8]. Undoped  $\text{LaMnO}_3$  is an insulator antiferromagnet with a cooperative Jahn–Teller (JT) distortion. Replacing a small amount of  $\text{La}^{3+}$  by  $\text{Sr}^{2+}$ , i.e., doping the compound with a small number of hole-like charge carriers, induces drastic changes in these properties. The cooperative JT effect is suppressed, ferromagnetism develops, metallic behavior is observed, and rhombohedral symmetry appears. Figure 1 shows the phase diagram for  $0 \leq x \leq 0.35$  between 250 and 500 K. As far as we are aware, there are no thermal transport measurements on these materials above room temperature. In this work thermal diffusivity measurements from 250 to 400 K are presented. The data reveal a dominant lattice contribution to thermal conductivity. The rather low values of the thermal diffusivity, indicating a phonon mean free path of the order of the lattice spacing, correlate with local distortion of the  $\text{MnO}_6$  octahedra. Modifications of the local structure are responsible for the anomalies at the magnetic and structural transitions. The critical behavior of the thermal diffusivity of the sample with  $x = 0.3$  at the ferromagnetic-to-paramagnetic transition has been studied. Although the sample shows a high rounding near the transition temperature, critical parameters close to the values predicted by the Ising model have been obtained ( $\alpha = 0.12$ ,  $A/A' = 0.80$ ).

## 2. EXPERIMENTAL PROCEDURES

Single crystals of  $\text{La}_{1-x}\text{Sr}_x\text{MnO}_3$  ( $x = 0, 0.05, 0.10, 0.125, 0.15, 0.165, 0.20, 0.25$ , and  $0.30$ ) were grown by the floating-zone technique. The polycrystalline seeds were prepared from a stoichiometric mixture of  $\text{La}_2\text{O}_3$ ,  $\text{SrCO}_3$ , and  $\text{Mn}_2\text{O}_3$  calcined and sintered at  $1200^\circ\text{C}$  for 72 h. Crystals were grown in an Ar-rich atmosphere at a pressure of 6 to 8 bar in order to reduce manganese evaporation. The nature of the crystal surface was checked by optical and scanning electron microscopy, while X-ray powder and Laue diffraction was used to assess the phase purity, structure, and crystalline quality. Surface images of polished cross sections of

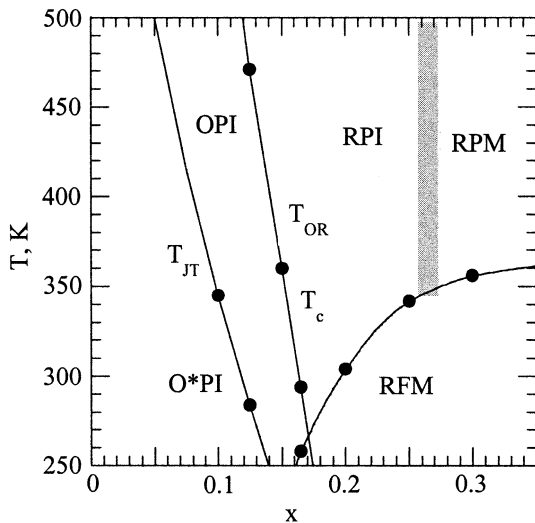


**Fig. 1.** Phase diagram for  $\text{La}_{1-x}\text{Sr}_x\text{MnO}_3$  ( $0 \leq x \leq 0.3$ ). O\*: Jahn-Teller distorted orthorhombic,  $c/\sqrt{2} < a, b$ ; O: orthorhombic,  $c/\sqrt{2} \approx a, b$ ; R: rhombohedral; P: paramagnetic; F: ferromagnetic; I: insulator; M: metal;  $T_{JT}$ : Jahn-Teller transition, and  $T_c$ : the Curie temperature. Dots represent measured data of this work.

**Table I.** Sample Parameters at Room Temperature

$x$	$a$ (nm)	$b$ (nm)	$c$ (nm)	$c/\sqrt{2}$	Symmetry	Space Group	Density ( $\text{g} \cdot \text{cm}^{-3}$ )
0.00	5.522	5.730	7.673	$< a, b$	O*	Pbnm	6.62
0.05	5.527	5.645	7.692	$< a, b$	O*	Pbnm	6.62
0.10	5.548	5.586	7.742	$< a, b$	O*	Pbnm	6.55
0.125	5.530	5.545	7.795	$\approx a, b$	O	Pbnm	6.54
0.15	5.505	5.544	7.790	$\approx a, b$	O	Pbnm	6.53
0.165	5.499	5.544	7.784	$\approx a, b$	O	Pbnm	6.53
0.30	5.511	5.511	13.367	—	R	$R\bar{3}c$	6.41

the crystals are smooth, with no evidence of micro-cracks, segregation, or twin boundaries. Detailed growing procedures were reported elsewhere [9]. Slices of thickness between 0.3 and 0.4 mm were cut from the grown crystals perpendicular to the growth direction ( $c$ -axis) for thermal diffusivity measurements. Their lattice parameters are given in Table I.

Thermal diffusivity measurements have been performed by a PPE setup in the standard back configuration [3]. A mechanically modulated He–Ne laser beam of 5 mW illuminates the upper surface of the sample under study. Its rear surface is in thermal contact with a 350  $\mu\text{m}$  thick  $\text{LiTaO}_3$  pyroelectric detector with Ni–Cr electrodes on both faces, by using a very thin layer of high vacuum silicone grease. The PPE signal is processed by a lock-in amplifier in the current mode. Both sample and detector are placed inside a nitrogen bath cryostat that allows measurements in the temperature range from 77 to 500 K, at rates that vary from 100  $\text{mK} \cdot \text{min}^{-1}$  for measurements over a wide temperature range to 10  $\text{mK} \cdot \text{min}^{-1}$  for high resolution runs close to the phase transitions. If the sample is opaque and thermally thick ( $\ell_s > \mu$ ), the natural logarithm and the phase of the normalized PPE voltage at a fixed temperature, i.e., the ratio of the voltage with and without a sample, are given by [3, 10]

$$\ln(V_n) = \ln \left( \frac{2 \frac{1-R_s}{1-R_p}}{1 + \frac{\epsilon_s}{\epsilon_p}} \right) - \frac{\ell_s}{\mu_s}, \quad (1)$$

$$\psi_n = -\frac{\ell_s}{\mu_s}, \quad (2)$$

where  $R$  is the optical reflection coefficient,  $\mu = \sqrt{D/(\pi f)}$  is the thermal diffusion length,  $D$  is the thermal diffusivity, and  $e$  is the thermal effusivity. Subscript indexes s and p refer to the sample and pyroelectric detector, respectively.

According to Eqs. (1) and (2), both the phase  $\psi_n$  and the natural logarithm  $\ln(V_n)$  of the PPE signal have a linear dependence on  $\sqrt{f}$ , with the same slope  $m$ , from which the thermal diffusivity of the sample can be determined,

$$D = \frac{\ell_s^2 \pi}{m^2}. \quad (3)$$

On the other hand, the temperature dependence of the thermal diffusivity can be measured as follows [10, 11]. First, we measure the thermal diffusivity  $D_{\text{ref}}$  at a fixed temperature  $T_{\text{ref}}$ , using the linear method explained above. Then we choose a frequency for which the sample is thermally thick. Finally we change the temperature while recording the phase of the PPE signal, first for the pyroelectric detector alone and then for the sample. If we define the phase difference as  $\Delta(T) = \psi_n(T) - \psi_n(T_{\text{ref}})$ , the temperature dependence of the thermal diffusivity is given by

$$D(T) = \left[ \frac{1}{\sqrt{D_{\text{ref}}}} - \frac{\Delta(T)}{\ell_s \sqrt{\pi f}} \right]^{-2}. \quad (4)$$

To calibrate our PPE setup we have measured the thermal diffusivity of  $\text{Cr}_2\text{O}_3$  across its magnetic phase transition.  $\text{Cr}_2\text{O}_3$  is a weakly anisotropic antiferromagnet with a Néel temperature  $T_N \approx 307$  K. The sample we have used is a 5 mm diameter disk with a thickness of 0.60 mm. Several measurements have been performed at frequencies of 12 and 23 Hz and at heating rates between 90 and 30  $\text{mK} \cdot \text{min}^{-1}$ , but no significant differences have been found. The temperature dependence of the thermal diffusivity is shown in Fig. 2a and agrees very well with the values previously reported by Marinelli and coworkers [4]. The sharpness of the dip of  $D$  at the transition indicates the good quality of the crystal as well as the high resolution of the PPE setup. In order to extract information on the critical parameters of  $\text{Cr}_2\text{O}_3$ , the experimental data of the inverse of  $D$  have been fitted to a function which is similar to the one used for specific heat [4, 12];

$$1/D = B + Ct + A|t|^{-\alpha} \left(1 + E|t|^{0.5}\right), \quad t > 0, \quad (5a)$$

$$1/D = B + Ct + A'|t|^{-\alpha} \left(1 + E'|t|^{0.5}\right), \quad t < 0, \quad (5b)$$

where  $t = (T - T_N)/T_N$  is the reduced temperature. As the thermal diffusivity is related to the specific heat  $c_p$  through the relation,

$$D = \frac{K}{\rho c_p}, \quad (6)$$

where  $K$  is the thermal conductivity and  $\rho$  is the density, the inverse of the thermal diffusivity has the same critical behavior as the specific heat, provided that the thermal conductivity does not change significantly, as is the case for  $\text{Cr}_2\text{O}_3$ . Moreover, fitting  $1/D$  instead of  $D$  itself is more appropriate because in the fit of  $D$  the critical exponent  $\alpha$  is always negative since the thermal diffusivity cannot diverge at  $T_N$ . On the contrary, the inverse of  $D$  has no restriction on the sign of  $\alpha$ . Accordingly, distinction between Heisenberg-like behavior ( $\alpha = -0.115$ ,  $A/A' = 1.521$ ) and Ising-like behavior ( $\alpha = 0.11$ ,  $A/A' = 0.524$ ) can be performed in a straightforward way. The temperature dependence of  $1/D$  close to the magnetic phase transition of  $\text{Cr}_2\text{O}_3$  is shown in Fig. 2b. The two branches have been simultaneously fitted to Eqs. (5). The parameters of the best fit are  $\alpha = -0.039$ ,  $A/A' = 1.27$  in perfect agreement with the result reported in Ref. 4 for the specific heat in the same temperature range, indicating that this material does not follow universal behavior.

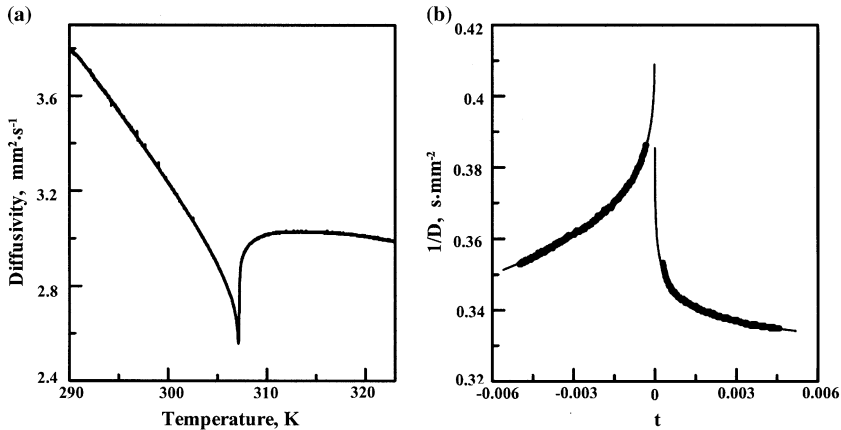


**Fig. 2.** (a) Temperature dependence of the thermal diffusivity of  $\text{Cr}_2\text{O}_3$  around the antiferromagnetic-to-paramagnetic phase transition. (b) Inverse of the thermal diffusivity versus the reduced temperature. Solid line corresponds to the best fit to Eq. (5).

### 3. EXPERIMENTAL RESULTS AND DISCUSSION

The temperature dependence of the thermal diffusivity along the  $c$ -axis of the  $\text{La}_{1-x}\text{Sr}_x\text{MnO}_3$  crystals is shown in Fig. 3. All of the  $D$  values are quite low for crystalline solids, with the data for lightly doped samples ( $x = 0.1$  to  $0.17$ ) near room temperature falling in the typical range of glasses ( $D = 0.4$  to  $0.8 \text{ mm}^2 \cdot \text{s}^{-1}$ ). Moreover, from the values of the specific heat and density the room temperature thermal conductivity can be calculated using Eq. (6). Its values are shown in Table II, and lie in the typical range of amorphous materials ( $0.5$  to  $5 \text{ W} \cdot \text{m}^{-1} \cdot \text{K}^{-1}$ ). On the other hand, from the values of the electrical resistivity  $r$  [7], the upper limit of the electronic contribution to the total thermal conductivity can be calculated using the Wiedemann–Franz law ( $K_e = L_o T/r$ ; where  $L_o = 2.45 \times 10^{-8} \text{ W} \cdot \Omega \cdot \text{K}^{-2}$  is the Lorentz number). Its values are also shown in Table II. As can be seen, the electronic contribution to the thermal conductivity is negligible even for the sample with  $x = 0.3$ , which exhibits a metallic behavior. Therefore, the heat conduction in these materials is due to phonons.

Kinetic theory provides the simplest model to express the thermal conductivity of a dilute gas  $K = \rho c_p \bar{v} \lambda / 3$ , where  $\bar{v}$  is the mean speed of the carriers and  $\lambda$  is their mean free path between collisions. This result has been extensively used to determine the mean free path in non-metallic materials where heat is carried entirely by phonons, as is the case for our

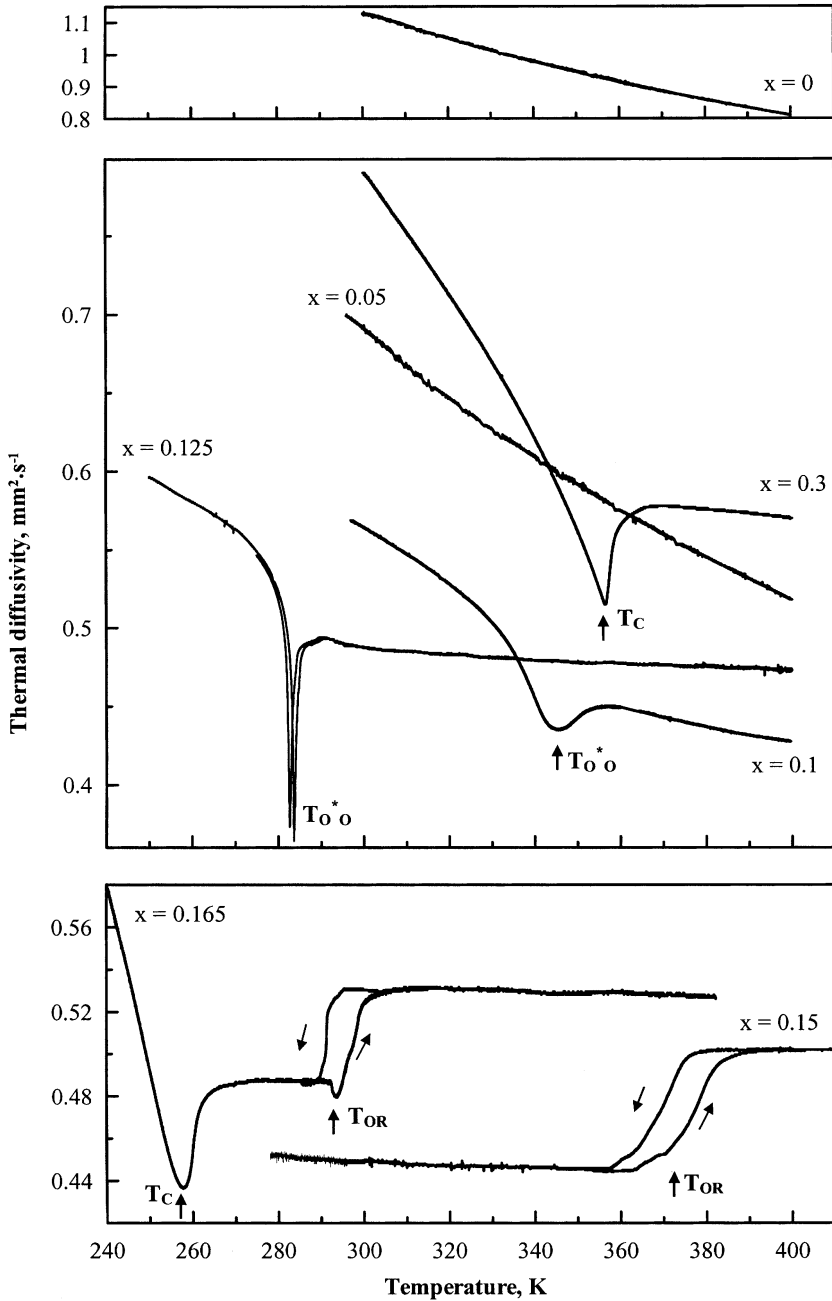


Fig. 3. Thermal diffusivity versus temperature for  $\text{La}_{1-x}\text{Sr}_x\text{MnO}_3$  single crystals.

**Table II.** Thermal Parameters at Room Temperature

$x$	$D$ ( $\text{mm}^2 \cdot \text{s}^{-1}$ )	$c_p^*$ ( $\text{J} \cdot \text{kg}^{-1} \cdot \text{K}^{-1}$ )	$K$ ( $\text{W} \cdot \text{m}^{-1} \cdot \text{K}^{-1}$ )	Resistivity <sup>a</sup> ( $\Omega \cdot \text{m}$ )	$K_e$ ( $\text{W} \cdot \text{m}^{-1} \cdot \text{K}^{-1}$ )
0.00	1.15	578	4.4	$2 \times 10^2$	$3 \times 10^{-8}$
0.05	0.77	600	3.1	10	$10^{-7}$
0.10	0.56	620	2.3	$10^{-2}$	$7 \times 10^{-4}$
0.125	0.47	594	1.8	$2 \times 10^{-3}$	$4 \times 10^{-3}$
0.15	0.45	620	1.8	$8 \times 10^{-4}$	0.01
0.165	0.52	608	2.1	$8 \times 10^{-4}$	0.01
0.30	0.90	575	3.3	$6 \times 10^{-5}$	0.12

<sup>a</sup> From Ref. 13.

samples. Substituting this expression into Eq. (6), an interpretation of the thermal diffusivity in terms of the scattering properties of the heat carriers is obtained,

$$D = \frac{1}{3} \bar{v} \lambda. \quad (7)$$

Since at room temperature  $\bar{v} \approx 3500 \text{ m} \cdot \text{s}^{-1}$  [13], the phonon mean free path for the undoped sample is about  $10 \text{ \AA}$ . As the Sr concentration increases,  $\lambda$  is reduced, reaching the minimum value of  $4 \text{ \AA}$  at  $x = 0.15$ , which is of the order of the distance between the Mn atoms. Higher Sr concentration produces an increase of  $\lambda$  up to  $8 \text{ \AA}$  at  $x = 0.3$ .

The thermal diffusivity far away from phase transitions decreases upon warming the sample (see Fig. 3). This is due to the fact that in an insulator  $\lambda$  is limited by the phonon-phonon scattering and should be a decreasing function of  $T$  or approach a constant value because of saturation at high temperatures.

The singularities of Fig. 3 correspond to the three kinds of phase transitions that these materials undergo in the temperature range of this study (see Fig. 1). Regarding the magnetic transition the samples with  $x = 0.165$  and  $x = 0.30$  experience a ferromagnetic-to-paramagnetic transition at  $T_c$  that is characterized by a dip in the thermal diffusivity. As in the case of the  $\text{Cr}_2\text{O}_3$  sample, the experimental data of  $1/D$  of  $\text{La}_{0.7}\text{Sr}_{0.3}\text{MnO}_3$  have been fitted to Eqs. (5). The results are shown in Fig. 4, where the open circles are the experimental data and the continuous line is the fit corresponding to the critical parameters  $\alpha = 0.12 \pm 0.01$  and  $A/A' = 0.80 \pm 0.15$ . From these values we can conclude that the behavior of this sample is close to that predicted by the Ising model, although the ratio of the critical amplitudes is higher than expected. Regarding the quality of the fit, it is clear from Figs. 2 and 4 that it is not as good as in



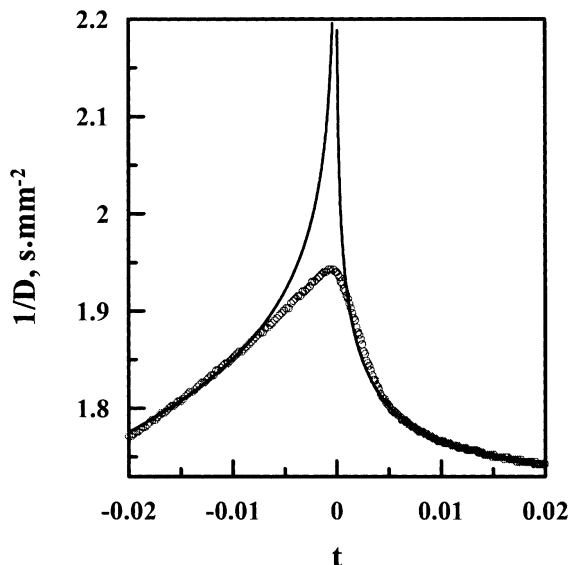


Fig. 4. Inverse of the thermal diffusivity of  $\text{La}_{0.7}\text{Sr}_{0.3}\text{MnO}_3$  versus the reduced temperature. Solid line corresponds to the best fit to Eq. (5).

the case of  $\text{Cr}_2\text{O}_3$ , which is in agreement with the  $\chi^2$  values:  $2.1 \times 10^{-6}$  for  $\text{La}_{0.7}\text{Sr}_{0.3}\text{MnO}_3$  and  $8.3 \times 10^{-8}$  for  $\text{Cr}_2\text{O}_3$ . It is worth noting that since the peak shows a pronounced rounding near the transition temperature, many points close to  $T_c$  have been suppressed in the fitting, reducing the reliability of the result, which has to be considered as a first approach. Actually rounding poses a severe constraint on the analysis of asymptotic behavior. This is due to the fact that thermal transport measurements depend strongly on the internal structure of the material and only extremely perfect single crystals can be used for investigation of critical behavior. In the case of the sample with  $x = 0.165$ , the rounding is so emphasized that the critical parameters cannot be obtained.

The structural transition between the JT distorted orthorhombic phase and the octahedron rotated orthorhombic phase ( $\text{O}^*\text{O}$ ) at  $T_{\text{JT}}$  shows a broad shallow minimum without hysteresis for the sample with  $x = 0.10$ , indicating its second-order nature; but there is a narrow and abrupt dip with a 1 K hysteresis in the sample with  $x = 0.125$ , showing its first-order nature. This change of the  $\text{O}^*\text{O}$  transition from second order to first order as  $T_{\text{JT}}$  approaches  $T_c$  has already been reported [7].

On the contrary, the structural transition from orthorhombic to rhombohedral (OR) at  $T_{\text{OR}}$  in the samples with  $x = 0.15$  and  $0.165$  is char-

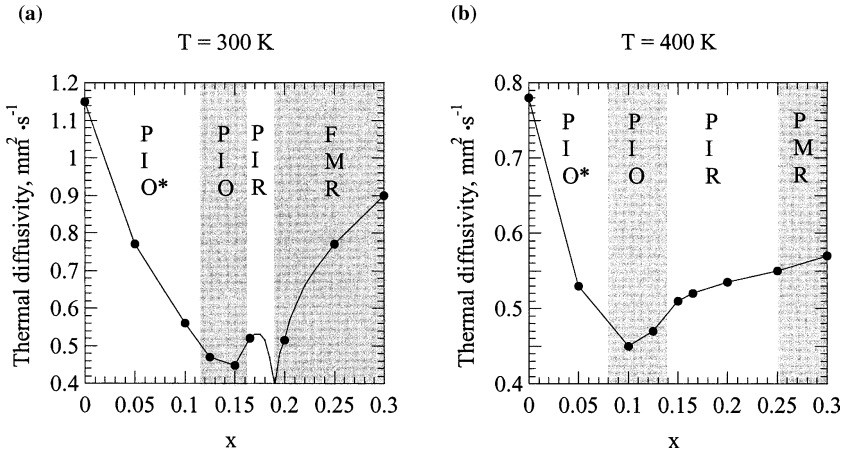


Fig. 5. Thermal diffusivity against Sr concentration at two temperatures: (a)  $T = 300$  K and (b)  $T = 400$  K. The continuous line is a guide for the eye.

acterized by a step with a 5 to 8% higher  $D$  at the rhombohedral phase. The 8 K hysteresis indicates the first-order nature of this transition. In the rhombohedral symmetry  $D$  remains constant over a wide range of temperature.

Figure 5 shows the evolution of the thermal diffusivity with the Sr concentration at room temperature and at 400 K. In both cases a drastic reduction of the phonon mean free path is observed for  $0.1 \leq x \leq 0.17$ . Then the thermal diffusivity increases as the Sr concentration does, but without reaching the value of the undoped sample. A similar behavior for the thermal conductivity at 50 K has already been reported [14]. There, the reduction of the thermal conductivity was ascribed to the crossover from localized to itinerant electrons associated with the insulator-to-metal transition. However, in the room temperature results of Fig. 5a three phase transitions (O $\rightarrow$ R, P $\rightarrow$ F, I $\rightarrow$ M) take place in a short  $x$  range, and therefore, it is difficult to explain the reason for this rise in diffusivity. In order to overcome this limitation, measurements at 400 K are shown in Fig. 5b. At this temperature there are only two phase transitions (O $\rightarrow$ R, I $\rightarrow$ M) which, besides, are more separated. The results suggest that the rise in diffusivity as the Sr concentration increases is related to the structural change from the orthorhombic to the rhombohedral phase. This is also supported by the fact that in the samples where there is an O $\rightarrow$ R transition,  $x=0.15$  and  $0.165$ , there is a step-like rise in diffusivity as the temperature increases (see Fig. 3).

## ACKNOWLEDGMENTS

This work has been supported in part by the Ministerio de Ciencia y Tecnología through Research Grant No. MAT2002-04153-C02-01 (50% FEDER funds).

## REFERENCES

1. M. B. Salamon and M. Jaime, *Rev. Mod. Phys.* **73**:583 (2001).
2. E. Dagotto, T. Hotta, and A. Moreo, *Phys. Rep.* **344**:1 (2001).
3. M. Chirtoc, D. Dadarlat, D. Bicanic, J. S. Antoniow, and M. Egée, in *Progress in Photo-thermal and Photoacoustic Science and Technology*, Vol. 3, A. Mandelis and P. Hess, eds. (SPIE, Bellingham, Washington, 1997).
4. M. Marinelli, F. Mercuri, U. Zammit, R. Pizzoferrato, F. Scudieri, and D. Dadarlat, *Phys. Rev. B* **49**:9523 (1994).
5. J. Thoen and C. Glorieux, *Thermochimica Acta* **304/305**:137 (1997).
6. Y. Moritomo, A. Asamitsu, and Y. Tokura, *Phys. Rev. B* **56**:12190 (1997).
7. G.-L. Liu, J.-S. Khou, and J. B. Goodenough, *Phys. Rev. B* **64**:144414 (2001).
8. J. Hemberger, A. Krimmel, T. Kurz, H.-A. Krug von Nidda, V. Yu. Ivanov, A. A. Mukhin, A. M. Balbashov, and A. Loidl, *Phys. Rev. B* **66**:094410 (2002).
9. D. Prabhakaran, A. I. Coldea, A. T. Boothroyd, and S. J. Blundell, *J. Crystal Growth* **237-239**:806 (2002).
10. A. Salazar, *Rev. Sci. Instrum.* **74**:825 (2003).
11. S. Delenclos, M. Chirtoc, A. Hadj Sahraoui, C. Kolinsky, and J. M. Buisine, *Rev. Sci. Instrum.* **73**:2773 (2002).
12. A. Kornblit and G. Ahlers, *Phys. Rev. B* **11**:2678 (1975).
13. Kh. G. Bogdanova, A. R. Bulatov, V. A. Golenishchev-Kutuzov, L. V. Elokhina, A. V. Kapralov, A. V. Korolev, E. A. Neifel'd, and M. M. Shakirzyanov, *Physics of the Solid State* **45**:298 (2003).
14. J. S. Zhou and J. B. Goodenough, *Phys. Rev. B* **64**:024421 (2001).